J|A|C|S
ARTICLES
Published on Web 09/02/2004

The Hydrophilic Phosphatriazaadamantane Ligand in the Development of H_2 Production Electrocatalysts: Iron Hydrogenase Model Complexes

Rosario Mejia-Rodriguez, Daesung Chong, Joseph H. Reibenspies, Manuel P. Soriaga, and Marcetta Y. Darensbourg*

Contribution from the Department of Chemistry, Texas A&M University, College Station, Texas 77843

Received November 3, 2003; E-mail: marcetta@mail.chem.tamu.edu

Abstract: As functional biomimics of the hydrogen-producing capability of the dinuclear active site in [Fe]-H_2ase, the Fe^IFe^I organometallic complexes, (μ-pdt)[$Fe(CO)_2$PTA]$_2$, **1-PTA$_2$**, (pdt = $SCH_2CH_2CH_2S$; PTA = 1,3,5-triaza-7-phosphaadamantane), and (μ-pdt)[$Fe(CO)_3$][$Fe(CO)_2$PTA], **1-PTA**, were synthesized and fully characterized. For comparison to the hydrophobic (μ-pdt)[$Fe(CO)_2(PMe_3)]_2$ and $\{(\mu\text{-H})(\mu\text{-pdt})[Fe(CO)_2(PMe_3)]_2\}^+$ analogues, electrochemical responses of **1-PTA$_2$** and **1-(PTA·H$^+$)$_2$** were recorded in acetonitrile and in acetonitrile/water mixtures in the absence and presence of acetic acid. The production of H_2 and the dependence of current on acid concentration indicated that the complexes were solution electrocatalysts that decreased over-voltage for H^+ reduction from HOAc in CH_3CN by up to 600 mV. The most effective electrocatalyst is the asymmetric **1-PTA** species, which promotes H_2 formation from HOAc (pK_a in CH_3CN = 22.6) at −1.4 V in CH_3CN/H_2O mixtures at the Fe^0Fe^I redox level. Functionalization of the PTA ligand via N-protonation or N-methylation, generating (μ-pdt)[$Fe(CO)_2$(PTA-H^+)]$_2$, **1-(PTA·H$^+$)$_2$**, and (μ-pdt)[$Fe(CO)_2$(PTA-CH_3^+)]$_2$, **1-(PTA-Me$^+$)$_2$**, provided no obvious advantages for the electrocatalysis because in both cases the parent complex is reclaimed during one cycle under the electrochemical conditions and H_2 production catalysis develops from the neutral species. The order of proton/electron addition to the catalyst, i.e., the electrochemical mechanism, is dependent on the extent of P-donor ligand substitution and on the acid strength. Cyclic voltammetric curve-crossing phenomena was observed and analyzed in terms of the possible presence of an η^2-H_2−$Fe^{II}Fe^I$ species, derived from reduction of the Fe^IFe^I parent complex to Fe^0Fe^I followed by uptake of two protons in an ECCE mechanism.

Introduction

As structural and functional analogues of the active site of iron-only hydrogenase, [Fe]H_2ase, dinuclear iron complexes (μ-pdt)[$Fe(CO)_2L]_2$ (pdt = $-SCH_2CH_2CH_2S-$; L = PMe_3, CN^-, and CO) have been shown to serve as electrocatalysts for H_2 production.[1−3] Features in common with the biological catalyst include the terminal diatomic ligand CO, a short Fe−Fe distance, and a bidentate, chelating dithiolate that bridges two Fe^I centers in a butterfly structure.[4] Since PMe_3 has an electron-donating ability similar to that of the biologically relevant CN^-, without the complicating nucleophilic reactivity of the cyanide nitrogen, the phosphine derivative has also been used in electrochemical and electrocatalysis studies.[1−3]

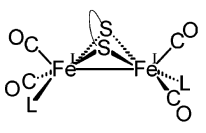

model complexes

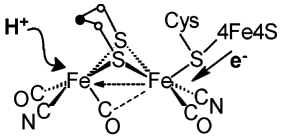

Fe-H_2ase active site [5,6,7]

Our work has focused on the CO and PMe_3 derivatives in studies of the effect of the ligand, the dithiolate bridge, and the S-to-S linker on electrocatalysis, examples of which are provided in Figure 1.[3] Such compounds are only soluble in organic solvents, and electrochemical and electrocatalytic studies were carried out in CH_3CN solution, using a glassy carbon electrode and a weak acid, HOAc, as proton source. Characterization of H_2 as the gas liberated was by ^{1}H NMR spectroscopy in gas-purged CD_2Cl_2 solutions. Electrochemical responses typical of electrocatalysis were observed at very negative potentials of −1.75 to −1.91 V, thus reducing the electropotential for HOAc reduction by up to 0.4 V. That is, under the same conditions in CH_3CN with no electrocatalyst, HOAc at 100 mM concentration is reduced to H_2 at −2.2 V, well within the acetonitrile solvent window (which extends past −2.5 V, Figure 1d). For the all-CO complex, the first reduction event at −1.34 V (Figure 1a) assigned by IR spectroelectrochemistry to the $Fe^IFe^I \rightarrow Fe^IFe^0$ process was not catalytically active.[3] Dihydrogen was, however, produced catalytically at −1.95 V, which is the second reduction, the $Fe^IFe^0 \rightarrow Fe^0Fe^0$ process. For the all-CO complex,

(1) Gloaguen, F.; Lawrence, J. D.; Rauchfuss, T. B. *J. Am. Chem. Soc.* **2001**, *123*, 9476−9477.
(2) Gloaguen, F.; Lawrence, J. D.; Rauchfuss, T. B.; Bénard, M.; Rohmer, M.-M. *Inorg. Chem.* **2002**, *41*, 6573−6582.
(3) Chong, D.; Georgakaki, I. P.; Mejía-Rodríguez, R.; Sanabria-Chinchilla, J.; Soriaga, M. P.; Darensbourg, M. Y. *J. Chem. Soc., Dalton Trans.* **2003**, 4158−4163.
(4) Darensbourg, M. Y.; Lyon, E. J.; Zhao, X.; Georgakaki, I. P. *Proc. Natl. Acad. Sci. U.S.A.* **2003**, *100*, 3683−3688.

10.1021/ja039394v CCC: $27.50

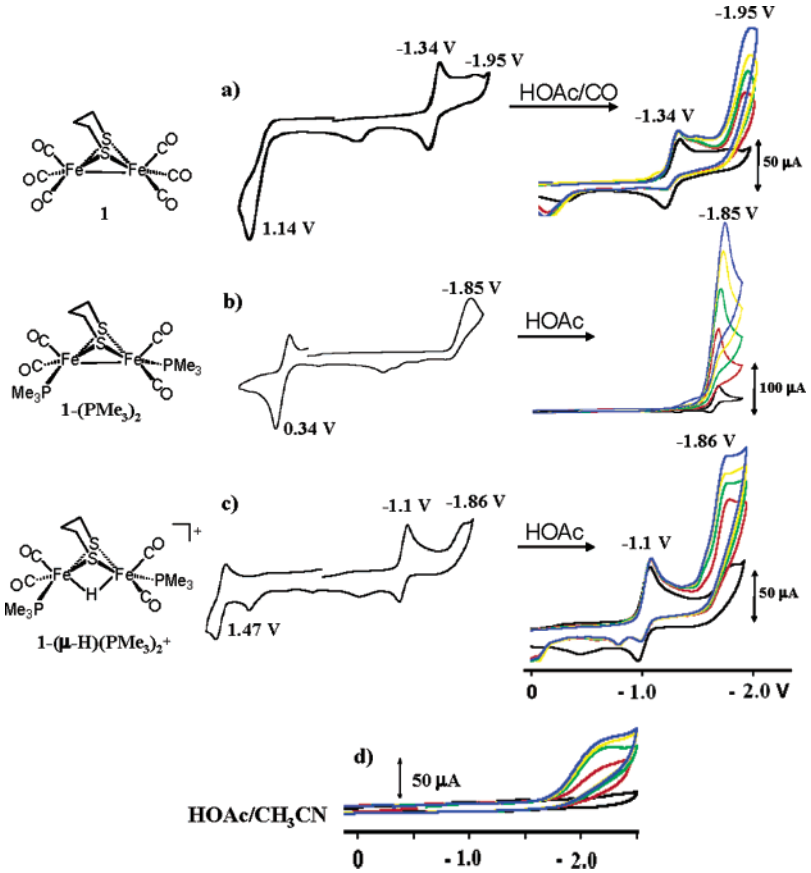

Figure 1. Cyclic voltammograms of neutral and monocationic complexes, 2.0 mM. (a) **1**,[3] (b) **1-(PMe$_3$)$_2$**, (c) **1-(*μ*-H)(PMe$_3$)$_2^+$** with HOAc (0, 25, 50, 75, and 100 mM), and (d) CH_3CN with added glacial HOAc (25, 50, 75, and 100 mM) in CH_3CN solution with electrochemical parameters as described in Table 2.

Scheme 1. Proposed Mechanisms for H_2 Production from (*μ*-pdt)[Fe(CO)$_2$L]$_2$ Model Complexes[a]

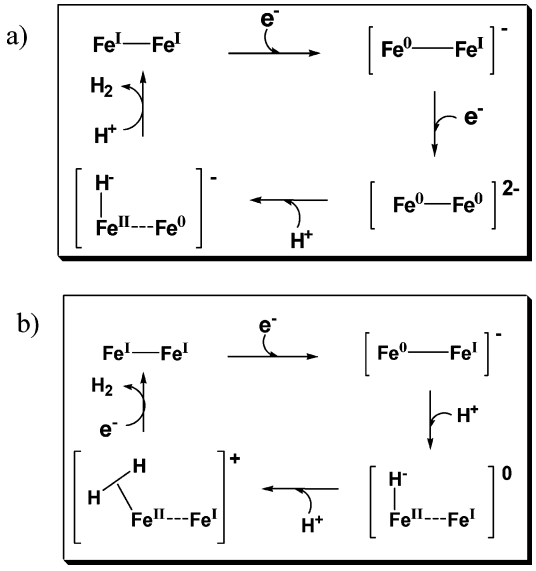

[a] (a) EECC, L = CO. (b) ECCE, L = phosphine.

the electrochemical measurements were made in CO-saturated solutions to inhibit CO dissociation from the labile Fe^IFe^0 radical anion. Thus, the addition of two electrons to the intact, all-CO complex preceded addition of two protons in an EECC electrochemical mechanism (Scheme 1a). In contrast, the doubly substituted bisphosphine complex catalyzed H_2 production from HOAc in CH_3CN at its first reduction event (and only reduction within the CH_3CN solvent window), assigned to $Fe^IFe^I \rightarrow Fe^IFe^0$, which takes place at −1.85 V. The ECCE mechanism in Scheme 1b is a likely possibility for the reaction path.[3]

Strong acids protonate the (*μ*-pdt)[Fe(CO)$_2$PMe$_3$]$_2$ complex, generating the cationic bridging hydride complex, (*μ*-H)(*μ*-pdt)-[Fe(CO)$_2$PMe$_3$]$_2^+$.[8] As shown in Figure 1c, two reduction events are characteristic of this complex; only the more negative, which corresponds to the neutral (*μ*-pdt)[Fe(CO)$_2$PMe$_3$]$_2$, is involved in electrocatalysis of H_2 production with HOAc. However, with the strong acid trifluoromethanesulfonic acid, or triflic acid (vide infra), the first reduction event is also electrocatalytically active.[2] A mixed ligand system, (*μ*-pdt)[Fe(CO)$_2$PMe$_3$][Fe(CO)$_2$CN]$^-$, was reported by Rauchfuss et al. to evolve hydrogen at a potential of −1 V in the presence of strong acids.[1,2] The exact order of the uptake of two protons and two electrons by the catalysts remains to be established but most certainly involves initial protonation of the cyanide ligand in either CECE or CCEE mechanisms.

In none of these preliminary explorations of the H_2-evolving capabilities of such [Fe]H_2ase biomimetic complexes is the coordination geometries or precise nature of the intermediate species known. However, it is clear that the diiron organometallics offer various possibilities for electrochemical reaction

(5) Peters, J. W.; Lanzilotta, W. N.; Lemon, B. J.; Seefeldt, L. C. *Science* **1998**, *282*, 1853−1858.
(6) Nicolet, Y.; Piras, C.; Legrand, P.; Hatchikian, C. E.; Fontecilla-Camps, J. C. *Structure* **1999**, *7*, 13−23.
(7) Nicolet, Y.; De Lacey, A. L.; Vernéde, X.; Fernandez, V. M.; Hatchikian, E. C.; Fontecilla-Camps, J. C. *J. Am. Chem. Soc.* **2001**, *123*, 1596−1601.
(8) Zhao, X.; Georgakaki, I. P.; Miller, M. L.; Yarbrough, J. C.; Darensbourg, M. Y. *J. Am. Chem. Soc.* **2001**, *123*, 9710−9711.

pathways dependent on proton source (acid strength) and reduction potential (electron availability or "strength").[9]

The [Fe]H_2ase enzyme generates H_2 at neutral pH values and at potentials of ca. −400 mV in a protein matrix with an unknown number of water molecules near the active site.[10,11] Therefore, the quest for H_2 production by synthetic analogues must balance acid strength and reduction potential, with the ultimate goal of finding catalysts that facilitate mild conditions of both proton and electron sources. To achieve this, knowledge of the molecular process(es), including the factors that influence the stability of Fe^0Fe^I radical anions, the hydrogenic species, Fe^{II}−H or $Fe^{II}(\eta^2$-$H_2)$, and the barriers to their formation, are critical issues to be addressed. On the basis of the particular dinuclear system described above, modifications can be made in the substituent ligand to improve hydrophilicity, and possibly water solubility, as well as to test the effect of complex charge on the redox potential. This we have approached with the complexes (μ-pdt)[$Fe(CO)_3$][$Fe(CO)_2$PTA], **1-PTA**, and (μ-pdt)-[$Fe(CO)_2$PTA]$_2$, **1-PTA$_2$**, (PTA = 1,3,5-triaza-7-phosphaadamantane = $P(CH_2)_6N_3$), and protonated and methylated derivatives, **1-(PTA·H$^+$)$_2$** and **1-(PTA-Me$^+$)$_2$**.

Experimental Section

Materials and Techniques. Solvents were of reagent grade and purified as follows: Dichloromethane was distilled over P_2O_5 under N_2. Acetonitrile was distilled once from CaH_2, once from P_2O_5, and freshly distilled from CaH_2. Diethyl ether, hexane, and THF were distilled from sodium/benzophenone under N_2. The parent (μ-pdt)$Fe_2(CO)_6$, **1**, and 1,3,5-triaza-7-phosphaadamantane (PTA), were prepared according to literature methods.[12,13] The following materials were of reagent grade and used as received: $Fe_3(CO)_{12}$, 1,3-propanedithiol, $CF_3SO_3CH_3$, concentrated HCl and NH_4PF_6 (Aldrich Chemical Co.), and deuterated solvents (Cambridge Isotope Laboratories).

Infrared spectra were recorded on an IBM IR/32 using a 0.1-mm NaCl cell. ^{1}H and ^{31}P NMR (85% H_3PO_4 was used as external reference) spectra were recorded on a Unity+ 300 MHz superconducting NMR instrument operating at 299.9 and 121.43 MHz, respectively. Conductivity measurements were performed in an Orion 160 conductivity meter. Elemental analyses were carried out by Canadian Microanalytical Service in Delta, British Columbia, Canada. Mass spectral analyses were done at the Laboratory for Biological Mass Spectroscopy at Texas A&M University. Electrospray ionization mass spectra were recorded using an MDS-Series QStar Pulsar with a spray voltage of 5 keV.

Preparation of (μ-pdt)[$Fe(CO)_2$PTA]$_2$, 1-PTA$_2$. To the red solution of (μ-pdt)$Fe_2(CO)_6$ (0.602 g, 1.56 mmol) in CH_3CN (25 mL) was added via cannula the PTA solution (0.503 g, 3.20 mmol, dissolved in 12 mL of MeOH). The reaction mixture was refluxed until IR spectroscopy indicated there was no remaining carbonyl complex starting material. After solvent removal in a vacuum, the solid residue was washed twice with 15−20-mL portions of dry degassed hexanes. An orange solid was obtained in nearly quantitative yield. Crystals suitable for X-ray analysis were grown from a layered methanol−hexanes solution. IR (ν(CO) region in CH_3CN, cm^{-1}): 1986 (w), 1953 (s), 1907 (m). ^{1}H NMR (ppm, acetone-d_6): 4.51 (s, 6 H), 4.13 (s, 6H), 1.99 (t, 4 H, SCH_2, J = 5.9 Hz), 1.77 (q, 2 H, CCH_2C, J = 5.9 Hz). ^{31}P NMR: −17.75 ppm. Elemental analysis found (calculated) %: C, 35.8 (35.4); H, 4.86 (4.69); N, 13.5 (13.0).

(μ-pdt)[$Fe(CO)_2$PTA][$Fe(CO)_3$], 1-PTA. The same procedure described above was followed with temperature maintained at ∼40 °C. After 20 h, the main product (ν(CO) IR monitor) was the monosubstituted complex **1-PTA** as a mixture with 5−10% of the parent hexacarbonyl complex and 5−10% disubstituted product, **1-PTA$_2$.** Further manipulations of this mixture were performed in air. Following solvent evaporation, the solids were dissolved in a minimum of THF for column chromatography on a 2.5 × 30 cm^2 silica gel column. Hexane was used to first elute the all-CO complex **1**, followed by THF to separate the PTA products. The **1-PTA** complex eluted first, and on concentration of the THF solution, orange, needle-shaped crystals of **1-PTA** were obtained. IR (ν(CO) region in CH_3CN, cm^{-1}): 2038 (s), 1983 (vs), 1963 (s), 1928 (m). ^{31}P NMR (CD_3CN): −18.4 ppm.

(μ-pdt)[$Fe(CO)_2$(PTA-H)]$_2$(PF_6)$_2$, 1-(PTA·H$^+$)$_2$. A 0.143-g sample of (μ-pdt)[$Fe(CO)_2$PTA]$_2$ (0.222 mmol) was dissolved in 13 mL of 0.1 M HCl, forming a reddish orange solution. An orange solid precipitated upon addition of a saturated aqueous solution of NH_4PF_6. After filtration and air-drying, 0.170 g of product (0.18 mmol, 80% yield) was obtained. IR (in CH_3CN, cm^{-1}): 2001 (w), 1969 (s), 1925 (m). ^{1}H NMR (ppm, acetone-d_6): 5.33 (s, 6 H), 4.79 (s, 6H), 2.11 (t, 4 H), 1.85 (q, 2 H). ^{31}P NMR: −3.88, −142.98 ppm (PF_6^-). Λ_M 263 ohm^{-1} cm^2 mol^{-1}. ESI mass spectrum: m/z = 645.0, {[(μ-pdt)[$Fe(CO)_2$(PTA-H)] [$Fe(CO)_2$PTA)]}$^+$.

(μ-pdt)[$Fe(CO)_2$(PTA-CH_3)]$_2$(CF_3SO_3)$_2$, 1-(PTA-Me$^+$)$_2$. On addition of 70 μL (0.102 g, 0.618 mmol) of $CF_3SO_3CH_3$ to a 10-mL CH_2Cl_2 solution containing 0.100 g (0.155 mmol) of **1-(PTA)$_2$**, a reddish-orange solid precipitated. After filtration in air, the solid was washed with CH_2Cl_2 and air-dried. IR (in CH_3CN, cm^{-1}): 2003 (w), 1970 (s), 1927 (m). ^{1}H NMR (CD_3CN): 1.77 (m, 2 H, CCH_2C), 2.06 (t, 4 H, SCH_2, J = 5.6 Hz), 2.74 (s, 6 H, NCH_3), complex set of peaks from δ 3.95 to δ 4.91 ppm (24 H). ^{31}P NMR: 1.68 ppm. Elemental analysis, found (calculated) %: C, 27.9 (28.4); H, 3.73 (3.73); N, 8.27 (8.64). Λ_M 275 ohm^{-1} cm^2 mol^{-1}. m/z = 822.99, {[(μ-pdt)[$Fe(CO)_2$(PTA-CH_3)]$_2$(CF_3SO_3)$_2$}$^+$.

X-ray Structure Determinations. The X-ray data were collected on a Bruker Smart 1000 CCD diffractometer and covered a hemisphere of reciprocal space by a combination of three sets of exposures. The space groups were determined on the basis of systematic absences and intensity statistics. The structures were solved by direct methods. Anisotropic displacement parameters were determined for all non-hydrogen atoms. Hydrogen atoms were placed at idealized positions and refined with fixed isotropic displacement parameters. The following is a list of programs used: for data collection and cell refinement, SMART;[14] data reduction, SAINTPLUS;[15] structure solution, SHELXS-97 (Sheldrick);[16] structure refinement, SHELXL-97 (Sheldrick);[17] and molecular graphics and preparation of material for publication, SHELXTL-Plus, version 5.1 or later (Bruker).[18] Crystallographic data are listed in Supporting Information.

Electrochemistry. Measurements were made using a BAS 100A electrochemical workstation. All voltammograms were obtained in a conventional and a gastight three-electrode cell under N_2 or CO atmosphere and room temperature. The working electrode was a glassy carbon disk (0.071 cm^2) polished with 1-μm diamond paste and sonicated for 15 min prior to use. The supporting electrolyte was 0.1 M n-Bu_4NBF_4. The experimental reference electrode was Ag/Ag^+ prepared by anodizing a silver wire in an CH_3CN solution of 0.01 M $AgNO_3$/0.1 M n-Bu_4NBF_4. All potentials are reported relative to the normal hydrogen electrode (NHE) using Cp_2Fe/Cp_2Fe^+ as reference

(9) Collman, J. P.; Ha, Y.; Wagenknecht, P. S.; Lopez, M−A.; Guilard, R. *J. Am. Chem. Soc.* **1993**, *115*, 9080−9088.
(10) Holm, R. H.; Kennepohl, P.; Solomon, E. I. *Chem. Rev.* **1996**, *96*, 2239−2314.
(11) Butt, J. N.; Filipiak, M.; Hagen, W. R. *Eur. J. Biochem.* **1997**, *245*, 116−122.
(12) Lyon, E. J.; Georgakaki, I. P.; Reibenspies, J. H.; Darensbourg, M. Y. *J. Am. Chem. Soc.* **2001**, *123*, 3268−3278.
(13) Daigle, D. J. *Inorg. Synth.* **1998**, *32*, 40−45.
(14) *SMART 1000 CCD*; Bruker Analytical X-ray Systems: Madison, WI, 1999.
(15) *SAINT-Plus*, version 6.02; Bruker Analytical X-ray Systems: Madison, WI, 1999.
(16) Sheldrick, G. *SHELXS-97*: *Program for Crystal Structure Solution*; Institüt für Anorganische Chemie der Universität: Göttingen, Germany, 1986.
(17) Sheldrick, G. *SHELXL-97: Program for Crystal Structure Refinement*; Institüt für Anorganische Chemie der Universität: Göttingen, Germany, 1977.
(18) *SHELXTL*, version 5.1 or later; Bruker Analytical X-ray Systems: Madison, WI, 1998.

Table 1. Selected Metric Data for Binuclear Iron Phosphino Complexes

	1-(PMe$_3$)$_2$[8]	**1-PTA**	**1-PTA$_2$**
Fe−Fe (Å)	2.555(2)	2.542(2)	2.5535(6)
Fe−P	2.234(3)[a]	2.215(3)	2.2139(9)[a]
Fe−$C_{CO,ap}$[b]	1.772(9)	1.789(12)	1.776(4)
Fe−$C_{CO,ba}$	1.742(10)	1.757(11)[c]	1.764(4)
Fe−$S_{\mu-SR}$[d] (Å)	2.254(2)	2.264(3)	2.258(9)
Fe disp[e] (Å)	0.376	0.395	0.389
S···S	3.026	3.050	3.051
dihedral ∠(deg)[f]	109.2	108.4	106.8
Fe−S−Fe ∠(deg)	69.06(8)	68.29(9)	68.85(3)
S−Fe−S ∠(deg)	84.34(11)	84.66(10)	84.98(3)

[a] Average of two Fe−P_{ba} bonds. [b] Average of two Fe−$C_{CO,ap}$ bonds. [c] Average of three Fe−$C_{CO,ba}$ bonds. [d] Average of four Fe−$S_{\mu-SR}$ bonds. [e] Fe disp = displacement of Fe from best plane of $S_2L_{2(ba)}$ toward L_{ap}. [f] Defined by the intersection of the two Fe_2S planes.

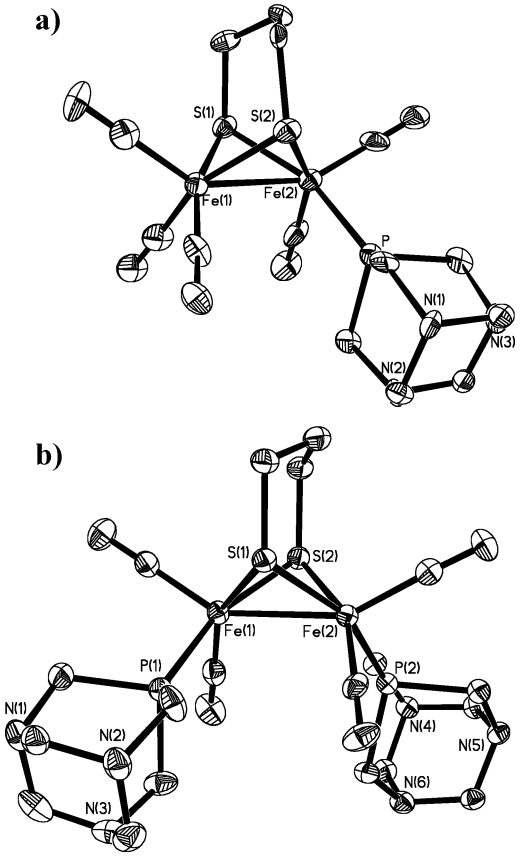

Figure 2. Thermal ellipsoid representations (50% probability) of the molecular structures of (a) **1-PTA** and (b) **1-PTA$_2$**.

(the literature value for $E_{1/2}^{NHE} = 0.40$ V in CH_3CN).[19] The counter electrode was platinum wire. Bulk electrolyses for electrocatalytic reactions were carried out under N_2 atmosphere using an EG&G model 273 Potentiostat and Galvanostat or BAS 100A Potentiostat. Electrocatalytic experiments were run for 1 h on a vitreous carbon rod (A = 3.34 cm^2) in a two-compartment, gastight, H-type electrolysis cell containing ca. 20 mL of CH_3CN, which was 5.0 mM in the diiron PTA derivatives and 0.1 M in n-Bu_4NBF_4. Increments of glacial acetic acid (up to 100 mM) were added by microsyringe. The solutions electrolysis were carried out under hydrodynamic conditions, vigorously stirring the solutions, to mitigate mass transport complications.

***In Situ* IR Spectroscopy. Spectroelectrochemistry.** *In situ* IR monitoring experiments during the course of bulk electrolysis were performed by use of a ReactIR 1000 equipped with an MCT detector

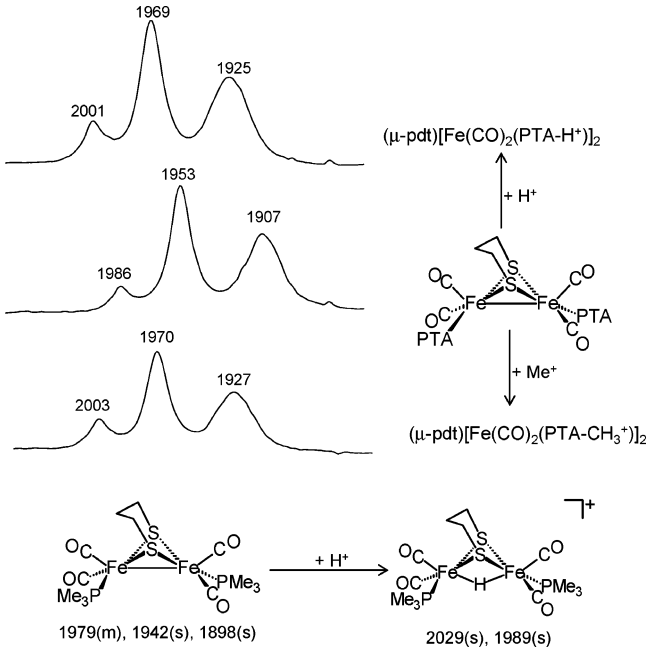

Figure 3. Infrared spectra (ν(CO) region, CH_3CN solution) demonstrating ligand-based reactivity with electrophiles versus binuclear oxidative addition of H^+ to Fe^I−Fe^I.

and 30-bounce SiCOMP *in situ* probe, which was purchased from Applied Systems Inc. A single-compartment cell that contained ca. 35-mL solutions was employed for the *in situ* infrared spectral measurements; this type of cell is suitable for noncoulometric measurements or for irreversible reactions.[3] The infrared spectrochemistry experiment for complex **1-(PTA-Me$^+$)$_2$** in CH_3CN/H_2O (3:1, v/v) mixtures was conducted on nonelectrolyzed solutions. The EPR spectrum was recorded on a Bruker X-band EPR spectrometer (model ESP 300E) with Oxford liquid helium/nitrogen cryostat at 10 K, 1 mW power, and 0.1 mT modulated amplitude.

Results and Discussion

The 1-PTA$_2$ and 1-PTA Complexes. The synthesis and isolation of the PTA complexes are described in the Experimental Section. Both **1-PTA$_2$** and **1-PTA** are air and thermally stable, in contrast to the mildly air-sensitive **1-(PMe$_3$)$_2$** complex.[8] The PTA derivatives are very soluble in THF and CH_2Cl_2 and are somewhat less soluble in acetone, MeOH, and CH_3CN. Their water solubility is poor but increases with decreasing pH. Solubility is enhanced in mixtures of water and organic solvents.

Molecular Structures. Complexes **1-PTA** and **1-PTA$_2$** crystallize in solvate-free forms in the $P2(1)/n$ and $P2(1)/c$ space groups, respectively, each with four molecules per unit cell. Selected metric data are compared in Table 1. Shown in Figure 2 as thermal ellipsoid plots, the molecular structures find the PTA ligands in the basal positions of the thiolate-edge-bridged, square-pyramidal iron species. As in other (μ-pdt)[$Fe(CO)_2L]_2$, L = PMe_3 and PMe_2Ph, the PTA ligands of **1-PTA$_2$** are transoid to each other.[8,20] This arrangement minimizes PTA ligand steric interactions with each other and with the propane−dithiolate bridge. Steric interactions produce the opposite orientation of phosphine-substituted (μ-$SR)_2[Fe(CO)_2L]_2$ complexes with R = Et or Me, in that the substituent phosphines adopt apical

(19) Gagné, R. R.; Koval, C. A.; Lisensky, G. C. *Inorg. Chem.* **1980**, *19*, 2854−2855.

(20) Zhao, X.; Georgakaki, I. P.; Miller, M. L.; Mejía-Rodríguez, R.; Chiang, C.-Y.; Darensbourg, M. Y. *Inorg. Chem.* **2002**, *41*, 3917−3928.

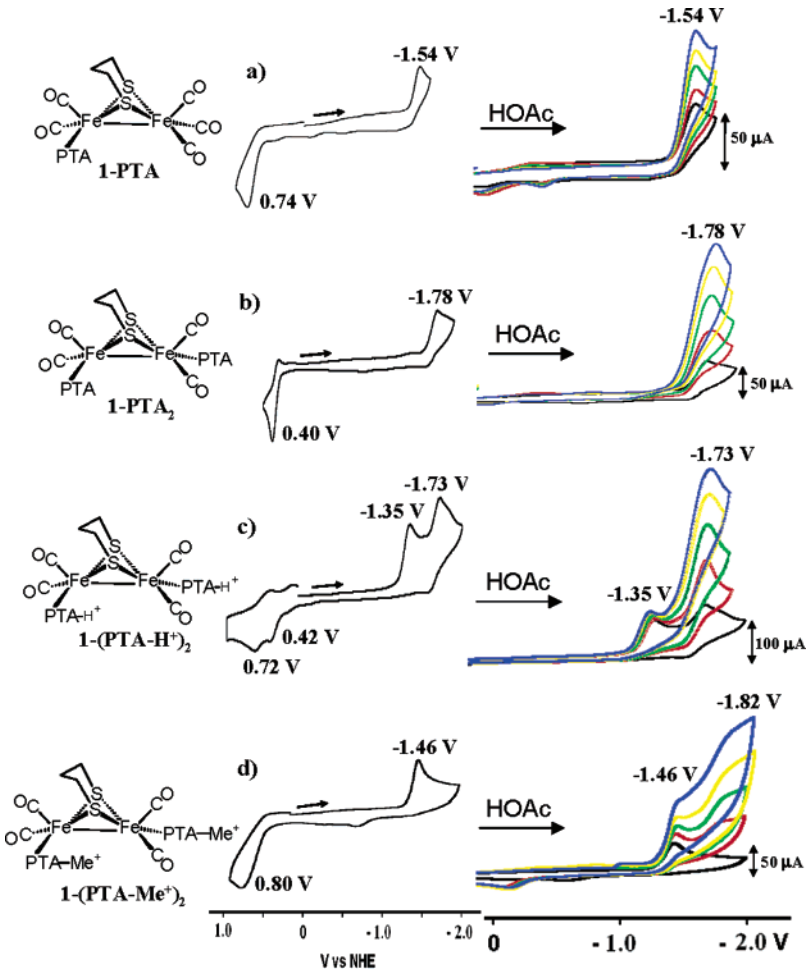

Figure 4. Cyclic voltammograms of neutral and dicationic complexes, 2.0 mM, in (a) **1-PTA**, (b) **1-PTA$_2$**, (c) **1-(PTA·H$^+$)$_2$**, and (d) **1-(PTA-Me$^+$)$_2$** with HOAc (0, 25, 50, 75, and 100 mM) in CH_3CN solution (0.1 M *n*-Bu_4NBF_4) with electrochemical parameters as described in Table 2.

positions in the $S_2Fe(CO)_2L$ square pyramids while the S−C bonds are in syn, outwardly directed, orientations. The Fe−Fe distance of 2.5535(6) Å in **1-PTA$_2$** is indistinguishable from that in (μ-pdt)[$Fe(CO)_2PMe_3$]$_2$, and there are no other differences of note in the metric parameters (Table 1).

While the ^{1}H NMR spectrum of **1-PTA** indicates rapid intramolecular proton site exchange in the propane−dithiolate C_3H_6 unit at room temperature, the solid-state X-ray structure finds that the boat form of the $Fe_2S_2C_3$ ring is on the $Fe(CO)_2PTA$ side of the diiron species; the chair form is on the $Fe(CO)_3$ side. There is no apparent consequence of this frozen conformation on metric data. The pseudo-square-pyramidal geometry about the iron atoms results in the usual displacement of iron out of the basal planes and toward the apical carbonyl. The average Fe_{displ} value for both **1-PTA$_2$** and **1-PTA** is 0.39 Å.

Donor Ability of PTA and Reactions of Diiron Derivatives with Acids. The three-band patterns in the ν(CO) IR spectra for the **1-(PMe$_3$)$_2$** and **1-PTA$_2$** complexes are nearly identical. The somewhat poorer donor ability of the latter is indicated by an average shift of 9 cm^{-1} to higher frequencies as compared to **1-(PMe$_3$)$_2$**. Both complexes react with excess hydrochloric acid, resulting in ionic salts that are obtained as precipitates upon Cl^-/PF_6^- ion exchange. Figure 3 presents the ν(CO) IR spectral monitor of these reactions. For **1-(PMe$_3$)$_2$**, the ν(CO) values of the neutral compound are shifted to higher values by ca. 70 cm^{-1}, indicating a drastic change in electron density about iron, consistent with the binuclear oxidative addition of a proton. The resultant bridging hydride complex, $Fe^{II}(\mu\text{-H})Fe^{II}$, has been thoroughly characterized by X-ray crystal structure and multinuclear NMR spectral analyses.[8,20] For the **1-PTA$_2$** complex, the ν(CO) band pattern of the protonated derivative, **1-(PTA·H$^+$)$_2$**, is identical to that of the neutral parent compound and the ν(CO) values are shifted by only 17 cm^{-1} on average. The small shift of the latter is consistent with ligand-based protonation as expected for the exposed tertiary nitrogen atoms on the PTA ligands.[21] Confirming this conclusion is ^{31}P NMR data, which show that the phosphorus of the iron-bound ligand experiences a significant downfield shift in the **1-(PTA·H$^+$)$_2$** species. Also supporting the assignment to a diprotonated species are conductivity measurements in 1.5 mM solutions in CH_3CN, $\Lambda_M = 263$ ohm^{-1} cm^2 mol^{-1}, which is within the range of a three-ion system[22] and consistent with the formulation {**1-(PTA·H$^+$)$_2$**}$^{2+}$ $(PF_6^-)_2$. Similar values were obtained for the product isolated from methylation of **1-PTA$_2$** with excess Me^+OTf^-.

Electrochemistry of PTA Derivatives of Diiron Complexes: Cyclic Voltammograms and Spectroelectrochemistry (IR Monitor and Assignments). The cyclic voltammograms

(21) (a) Fisher, K. J.; Alyea, E. C.; Shahnazarian, N. *Phosphorus, Sulfur Silicon* **1990**, *48*, 37−40. (b) Darensbourg, D. J.; Robertson, J. B.; Larkins, D. L.; Reibenspies, J. H. *Inorg. Chem.* **1999**, *38*, 2473−2481.
(22) Geary, W. J. *Coord. Chem. Rev.* **1971**, *7*, 81−122.

Table 2. Reduction Potentials[a] for PTA Derivatives of (μ-pdt)[Fe(CO)$_3$]$_2$ Complexes in CH_3CN and CH_3CN/H_2O at Ambient Temperature

complexes		E_{pc} vs NHE, V E_1 : $Fe^IFe^I \rightarrow Fe^0Fe^I$				
		CH_3CN		CH_3CN:H_2O, v/v		
		E_1	ton/h[b]	3:1	1:1	1:3
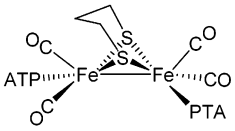	**1-PTA$_2$**	-1.78	16	-1.60	-1.57	-1.53
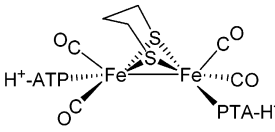	**1-(PTA•H$^+$)$_2$**	-1.35	—	-1.36	-1.34	-1.32
	"1-PTA$_2$"[c]	-1.73	21[d]	-1.62	-1.61	-1.59
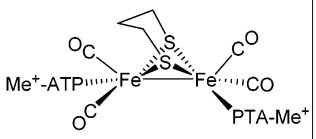	**1-(PTA-Me$^+$)$_2$**	-1.46	10[e]	-1.60	-1.61	-1.59
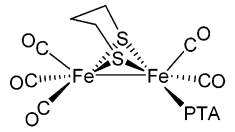	**1-PTA**	-1.54	7	-1.43	-1.40	-1.38

[a] CH_3CN solution (0.1 M *n*-Bu_4NBF_4) with a glassy carbon working electrode (A = 0.071 cm^2), referenced to NHE using Cp_2Fe/Cp_2Fe^+ standard ($E_{1/2}$ = 0.40 V).[19] Counter electrode: Pt. scan rate: 0.2 Vs^{-1}. H_2O solution (0.1 M KCl). μ-pdt = $-SCH_2CH_2CHS-$. [b] Ton = turnovers, ton/h determined as described in text. [c] Produced *in situ* from **1-(PTA·H$^+$)$_2$**. [d] Determined at −1.68 V. [e] Determined at −1.46 V.

shown in Figure 4 were recorded in CH_3CN solution; they were initiated from the rest potentials and proceed as indicated in the cathodic direction. Complexes **1-PTA**, **1-PTA$_2$**, and **1-(PTA-Me$^+$)$_2$** display an electrochemically irreversible reduction event at −1.54, −1.78, and −1.46 V, respectively. Bulk electrolysis demonstrated these events to be one-electron reduction processes, assigned to the $Fe^IFe^I + e^- \rightarrow Fe^IFe^0$ couple in each, analogous to the all-CO parent complex **1**.[3] In comparison to **1**, the Fe^IFe^I/Fe^IFe^0 couples of the **1-PTA** and **1-PTA$_2$** diiron complexes are negatively shifted, consistent with the increase in electron density about the two-iron core as a CO is replaced by the better donor phosphine ligand. The positive charge on the methylated-PTA derivative, **1-(PTA-Me$^+$)$_2$**, results in a smaller shift of the reduction potential; it is only 110 mV more negative than complex **1**. A summary of the reduction potentials in CH_3CN and in CH_3CN/H_2O mixtures is given in Table 2.

The doubly protonated PTA complex **1-(PTA·H$^+$)$_2$** exhibits two irreversible reduction events at −1.35 and −1.73 V (Figure 4). The assignment of the first event to a two-electron reduction process (eq 1) with formation of the neutral precursor is supported by coulometry and by *in situ* IR monitoring data as described below.

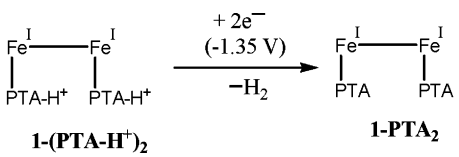

1-(PTA-H$^+$)$_2$ **1-PTA$_2$** **(1)**

Electrolysis of **1-(PTA·H$^+$)$_2$** at an applied potential of −1.47 V found a net consumption of 1.9 electrons per molecule. Because the potential of the second cathodic response was identical to the single reductive event of the parent **1-PTA$_2$** neutral complex, it was assumed to correspond to $(PTA)Fe^I-Fe^I(PTA) + e^- \rightarrow (PTA)Fe^I-Fe^0(PTA)$; controlled-potential coulometry established a net consumption of one electron at −1.78 V.

The *in situ* ReactIR spectroelectrochemical monitor of the infrared spectrum during the course of bulk electrolysis at an applied potential of −1.47 V over the course of 5 h showed a loss of intensity of the three ν(CO) IR bands of the dicationic starting material **1-(PTA·H$^+$)$_2$**, 1999, 1966, and 1924 cm^{-1}, with growth of bands at lower frequencies that match in intensity ratio and position those of the isolated and purified neutral **1-PTA$_2$**. Minor differences that were noted in the infrared spectra of the electrochemically generated species and the pure compound are due to the difference in instruments used to record the spectra, as well as the presence of electrolytes in the spectroelectrochemical monitor; a small band at 2040 cm^{-1} is of unknown origin. We note that electrochemical and electrocatalytic studies of the protonated species, isolated as the PF_6^- salt of **1-(PTA·H$^+$)$_2$** at negative potentials should give identical results as with the neutral **1-(PTA)$_2$** complex. In fact, as will be seen below, electropotential and electrocatalysis values are slightly different for isolated and purified **1-(PTA)$_2$** and that derived electrochemically in situ from the **1-(PTA·H$^+$)$_2$** precursor. Whether these slight differences are significant or are a measure of the inherent irreproducibility in the electrochemical studies is at present unknown.

Consistent with the spectroelectrochemical changes described above, the cyclic voltammograms of a solution containing the dicationic complex **1-(PTA·H$^+$)$_2$** displayed different electro-

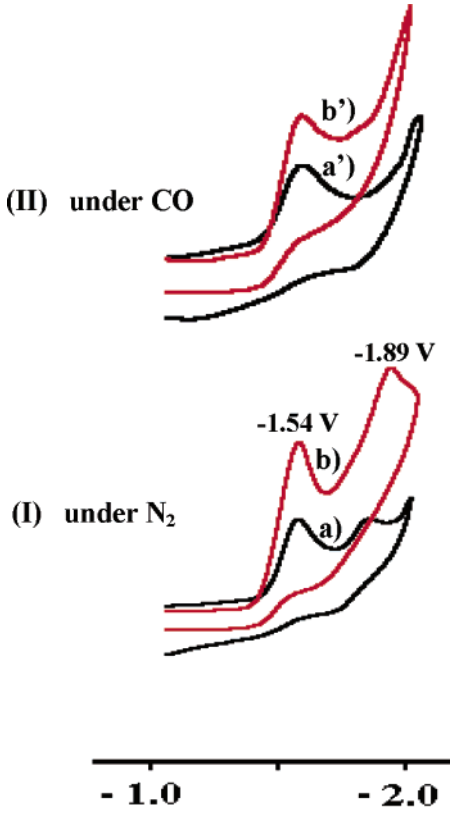

Figure 5. Cyclic voltammograms of **1-PTA** (2.0 mM) (Ia) under N_2 without HOAc and (Ib) with HOAc (25 mM), and cyclic voltammograms of **1-PTA** (2.0 mM) (IIa′) under CO without HOAc and (IIb′) with HOAc (25 mM) in CH_3CN (0.1 M *n*-Bu_4NBF_4) with electrochemical parameters as described in Table 2.

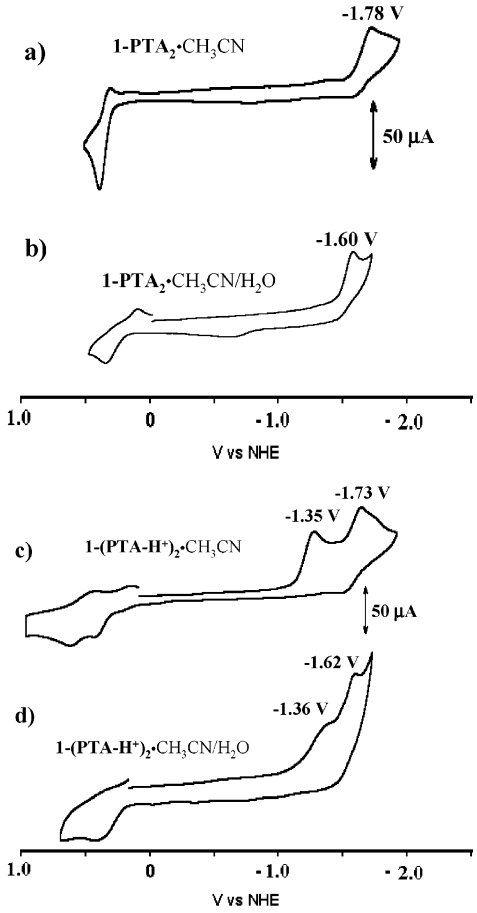

Figure 6. Cyclic voltammograms in CH_3CN solution (0.1 M *n*-Bu_4NBF_4) of (a) neutral **1-PTA$_2$** (2.0 mM) and (c) dicationic **1-(PTA·H$^+$)$_2$** (2.0 mM) complexes, and in CH_3CN (0.1 M *n*-Bu_4NBF_4)/H_2O (0.1 M KCl) = 3:1, v/v, of (b) neutral **1-PTA$_2$** (2.0 mM) and (d) dicationic **1-(PTA·H$^+$)$_2$** (2.0 mM) complexes with electrochemical parameters as described in Table 2.

chemical responses before and after bulk electrolysis at −1.47 V. After bulk electrolysis of the diprotonated complex only one reduction event remained, and its position at −1.75 V is indicative of the neutral complex **1-PTA$_2$** (−1.78 V).

It is instructive to compare the cyclic voltammograms of the diprotonated **1-PTA$_2$** with the monoprotonated bistrimethylphosphine analogue, (μ-pdt)[Fe(CO)$_2$PMe$_3$]$_2$. For the latter, for which protonation is metal based in binuclear oxidative addition (see Figure 3), the resultant $Fe^{II}Fe^{II}$-bridging hydride complex, (μ-H)(μ-pdt)[Fe(CO)$_2$PMe$_3$]$_2^+$, **1-(μ-H)(PMe$_3$)$_2^+$**, shows a quasi-reversible redox process at −1.1 V, assigned to the Fe^{II}-(μ-H)Fe^{II} + $e^- \rightleftharpoons Fe^{II}$($\mu$-H)$Fe^{II}$ redox couple (Figure 1c). An irreversible reduction at −1.86 V is similar in position and shape to the single irreversible reduction event at −1.85 V in the neutral PMe_3 complex, (μ-pdt)[Fe(CO)$_2$PMe$_3$]$_2$, **1-(PMe$_3$)$_2$**, (Figure 1b). For the latter, the reduction is confidently assigned to $Fe^IFe^I + e^- \rightarrow Fe^IFe^0$. Hence, we conclude the analogous waves at −1.86 V in solutions of **1-(μ-H)(PMe$_3$)$_2^+$** and at −1.75 V for **1-(PTA·H$^+$)$_2$** are due to the presence of the parent neutral complexes **1-(PMe$_3$)$_2$** and **1-PTA$_2$**, respectively. Both are produced by H-atom loss following reduction of the protonated species, regardless of the site of the protonation.[23]

The peak current of the redox couples described above is proportional to the square root of the scan rate (50−1000 mV s^{-1}), indicating that the electrochemical processes are diffusion-controlled.[24] Also observed for each PTA derivative is an irreversible oxidative event that is displaced positively by ca. 2.4 V for all species, tracking the reductive event (Figure 4). This oxidation is assumed to be due to the Fe^IFe^I/Fe^IFe^{II} couple, which experiences a greater stabilization by the better electron donor ability of the PTA ligand as compared to that of the all-CO neutral complex.

Electrocatalysis of H_2 Production in CH_3CN Solution. The current height of the single cathodic event at −1.78 V for **1-PTA$_2$** and at −1.54 V for **1-PTA**, derived from results in Figure 4, shows a linear dependence on the concentration of acetic acid. Only a minor increase in current height with added increments of acetic acid is observed for the redox wave at −1.35 V for **1-(PTA·H$^+$)$_2$**, while the second redox wave, at −1.73 V, shows a more significant electrocatalytic response (Figure 4c). That is, the greater acid sensitivity is derived from the more negative potential, which, in the case of the **1-(PTA·H$^+$)$_2$** species, is actually the reduction of the parent **1-PTA$_2$** produced *in situ* from the protonated species, **1-(PTA·H$^+$)$_2$**, *vide supra.*

Complex **1-(PTA-Me$^+$)$_2$** undergoes a one-electron irreversible reduction at −1.46 V, assigned to the $Fe^IFe^I \rightarrow Fe^IFe^0$ couple of the dicationic complex. The cyclic voltammograms of the **1-(PTA-Me$^+$)$_2$** in the presence of HOAc display two reduction waves at −1.46 and −1.82 V, respectively, in CH_3CN solution. The similarity of the latter event to the potential of the neutral **1-PTA$_2$** complex suggests degradation of the **1-(PTA-Me$^+$)$_2$** cation by demethylation.

(23) Koelle, U.; Ohst, S. *Inorg. Chem.* **1986**, *25*, 2689−2694.
(24) Brett C. M. A.; Brett, A. M. O. *Electrochemistry: Principles, Methods, and Applications*; Oxford University Press: Oxford, 1993.

In attempts to gain quantitative measures of the electrocatalytic activities of the PTA derivatives, controlled-potential electrolyses in a CH_3CN solution were performed as described in the Experimental Section. The electrolysis of complexes **1-PTA**, **1-PTA$_2$**, **1-(PTA·H$^+$)$_2$**, and **1-(PTA-Me$^+$)$_2$** (5 mM) at −1.60, −1.84, −1.79, and −1.52 V, respectively, in the presence of acetic acid (100 mM) consumes 14, 32, 42, and 20 electrons per molecule, respectively, per hour, corresponding to 7, 16, 21, and 10 turnovers per hour, respectively. These turnover numbers (TON) were obtained in the linear region of the coulogram where there is no evidence of catalyst degradation. A sample plot of such coulograms is provided in the Supporting Information.

A reasonable interpretation of these results is that reduction of the **1-PTA** and **1-PTA$_2$** derivatives initiates the electrocatalysis, followed by double protonation of the one-electron-reduced diiron species. A second reduction of an intermediate produces H_2, and the starting complex is reclaimed, as represented in the ECCE mechanism of Scheme 1.

Effect of Added CO. As compared to cyclic voltammograms of solutions under an atmosphere of N_2, CO-saturated CH_3CN solutions yielded simpler cyclic voltammograms for the all-CO diiron complexes.[3] Figure 1a shows that the two reduction events for (μ-pdt)$Fe_2(CO)_6$ solutions under CO atmosphere are separated by 600 mV. The more negative feature is assigned to the second reduction process, $Fe^IFe^0 \rightarrow Fe^0Fe^0$. As this reduction responds to added acid, it is concluded that this two-electron reduced level of the *intact*, all-CO species, [(μ-pdt)$Fe_2(CO)_6$]$^=$, is the electrocatalyst, and H_2 is evolved via an EECC mechanism (Scheme 1).

Given in Figure 4a is the cyclic voltammogram of the mono-PTA complex, **1-PTA**, in the absence and in the presence of HOAc, under N_2 atmosphere. Current enhancement is observed at the −1.54 V reduction potential, which corresponds to the $Fe^IFe^I \rightarrow Fe^IFe^0$. Figure 5 contrasts the extended-range (to −2 V) cyclic voltammogram of **1-PTA** under CO and under N_2. For the former, no further response that might be attributed to the second reduction, $Fe^IFe^0 \rightarrow Fe^0Fe^0$, is observed to the limit of measurement. Under N_2 (or Ar), both the −1.54 and an additional response at −1.89 V are observed. Because the addition of a second electron to **1-PTA** should be more difficult by ca. 600 mV and therefore be shifted to values more negative than −2.1 V, the response at −1.89 V is attributed to a solvent-substituted species, (μ-pdt)[$Fe(CO)_2$PTA][$Fe(CO)_2(NCCH_3)$] with oxidation state changes of $Fe^IFe^I \rightarrow Fe^IFe^0$. It should be noted that while the CO/CH_3CN ligand exchange occurs readily on **1-PTA** solutions exposed to intense sunlight, under ambient laboratory light, there is no significant exchange over many hours. Thus, the presence of the acetonitrile/PTA complex is likely to result from a radical chain reaction initiated by the production of the radical anion at the −1.54 V process. As has been well established for mononuclear 18-electron carbonyl complexes, loss of CO from the 19-electron radical anion results in subsequent uptake of an available ligand, which in our case is acetonitrile present as bulk solvent in large excess, followed by electron transfer to an all-CO species in a chain propagation step. Thus, there is a stabilizing effect of added CO on the **1-PTA** electrocatalysts.

Electrocatalysis in the Presence of Water. The addition of small amounts of water to acetonitrile containing **1-(μ-H)-(PMe$_3$)$_2$**$^+$ BF_4^- as solution electrocatalyst found no differences in H_2 production. While the water solubility of the diiron carbonyl complexes is increased by the presence of the hydrophilic PTA ligands, it is still insufficient for detailed electrochemical studies in pure water. However, in CH_3CN/H_2O mixtures the compounds show good solubility, and they are stable in a variety of CH_3CN and H_2O ratios (3:1, 1:1, and 1:3, v/v) for several hours. The electrochemical reduction processes of **1-PTA$_2$** and **1-PTA** in these mixed solvent systems are positively shifted, by ca. 100−250 mV (Table 2, Figure 6). For instance, the reduction potential of **1-PTA$_2$** moves to −1.60 V in CH_3CN/H_2O mixtures from −1.78 V in CH_3CN; optimal values are with the 3:1 CH_3CN/H_2O mixture. Among the possible reasons for this shift are pK_a lowering, H-bonding interactions to the N of the PTA ligand and product stabilization. It should be noted that our results and published data (using a Pt electrode)[25] find that the potential window for electrochemistry in CH_3CN/H_2O mixtures is +1.6 to ca. −1.7 V, and the observed events are within this window.

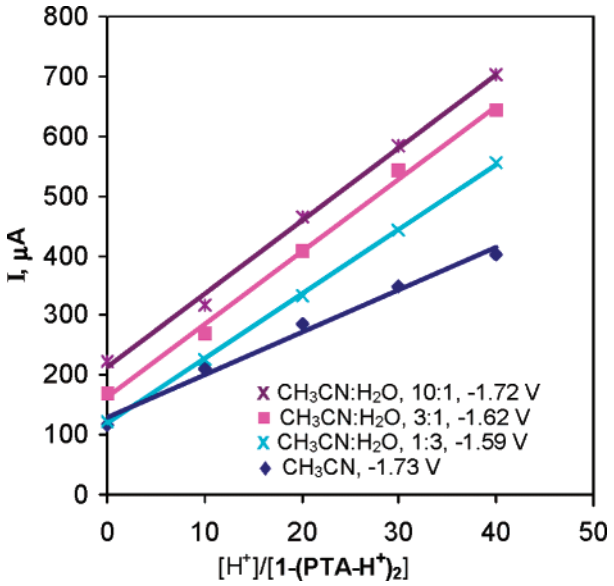

Figure 7. Dependence of current heights of electrocatalytic waves for **1-(PTA·H$^+$)$_2$** (2 mM) on acid concentration (0, 25, 50, 75, and 100 mM) in CH_3CN and CH_3CN/H_2O (10:1, 3:1, 1:1, and 1:3, v/v) mixed solvent systems.

Figure 7 presents plots of current vs acid concentration in pure CH_3CN and with varying CH_3CN/H_2O ratios for the electrocatalysis from the $Fe^IFe^I \rightarrow Fe^IFe^0$ couple of **1-PTA$_2$** (derived from {**1-(PTA·H$^+$)$_2$**}$^{2+}$). The steeper slopes in the presence of H_2O as compared to the pure CH_3CN solution are indicative of greater sensitivity of the reduced species to acid concentration. Enhanced sensitivity, i.e., greater catalytic activity, is seen with only 10% added water, even though the reduction potential is still at −1.72 V, i.e., roughly the same as that in pure CH_3CN. With a 3:1 CH_3CN/H_2O mixture, the reduction potential is shifted positively by ca. 100 mV, and the sensitivity to acid concentration is nearly as great as that of the 10:1 mixture. With greater water concentrations, the potential is invariant and the sensitivity appears to slightly decrease.

In contrast to **1-PTA$_2$** and **1-(PTA·H$^+$)$_2$**, the cyclic voltammogram of **1-(PTA-Me$^+$)$_2$** in CH_3CN shows a *negative* shift

(25) Tomita, Y.; Teruya, S.; Koga, O.; Hori, Y. *J. Electrochem. Soc.* **2000**, *147*, 4164−4167.

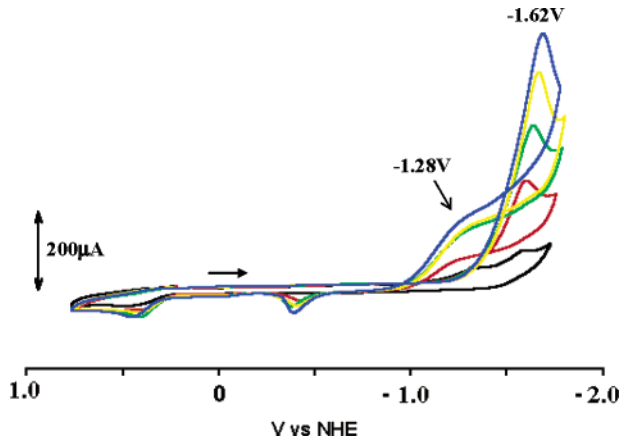

Figure 8. Cyclic voltammograms of **1-(PTA·H$^+$)$_2$** (2.0 mM) with HOAc (0, 25, 50, 75, and 100 mM) in CH_3CN (0.1 M *n*-Bu_4NBF_4)/H_2O (0.1 M KCl) = 3:1, v/v, with electrochemical parameters as described in Table 2.

of the cathodic event from −1.46 to −1.60 V in the presence of water (CH_3CN/H_2O 3:1) (Table 2). Because the more negative potential is the same as the reduction of the neutral complex **1-PTA$_2$** in the CH_3CN/H_2O mixture, we interpret the observation in terms of a demethylation of the quaternary nitrogen atom of the Fe−PTA-Me$^+$ moiety. That this demethylation is a chemical event, a result of degradation of the alkylated PTA ligand in the presence of the electrolytes, was confirmed by infrared spectral measurements on nonelectrolyzed solutions. Degradation of the methylated PTA complex **1-(PTA-Me$^+$)$_2$** was also found in CH_3CN solutions in the absence of water and in the presence of aliquots of glacial acetic acid, as shown in Figure 4d. While there is literature precedent for demethylation of quaternary ammonium salts (R_3MeN^+) by RSeH or RSH,[26] whether HOAc might be similarly effective is not known.

Occurrence and Significance of "Curve-Crossing". In the mixed CH_3CN/H_2O solvent system in the presence of HOAc a decidedly reproducible trace or curve-crossing was observed for **1-PTA$_2$** and **1-(PTA·H$^+$)$_2$** upon reversing the scan following the reduction at −1.62 V, resulting in the buildup of current response at −1.28 V.[27−29] (Although the **1-(PTA·H$^+$)$_2$** complex is at this potential in the form of **1-PTA$_2$**, solutions derived from it as precursor show more clearly defined curve-crossing phenomena. Acetonitrile solutions of **1-(PMe$_3$)$_2$** also demonstrate the curve-crossing event; however, in the earlier report, this observation was not analyzed.[3]) As such anomalies in cyclic voltammograms could result from instability of the metal complexes and deposition on the electrode, the following control studies were performed. Figure 8 shows, for the dicationic complex **1-(PTA·H$^+$)$_2$**, the current height of the −1.28 V event that appears in the reverse of the cathodic scan increases with increasing acid concentrations. Its dependence on potential scan rate, from 60 to 400 mV/s, was explored; at higher scan rates, pronounced ohmic-drop effects precluded a meaningful study. The results reveal a reproducible trend that as the scan rate was increased the peak currents of *both* the first and second ("curve-crossed") reduction reactions also increased. In addition, the "curve-crossed" response was *enhanced* relative to the major peak; that is, it was *not* diminished at the expense of the first peak. This observation provides evidence for an ECCE mechanism in which one of the C steps is rate-limiting; at higher scan rates, a larger fraction of the starting material is regenerated at reaction times that correspond to potentials positive of the "curve-crossing". The sweep-rate-dependence measurements likewise preclude surface deposition processes since those would be immediate and time-independent.

To further probe the possibility of the curve-crossing event arising from electrode deposition, cyclic voltammograms carried out with electrodes used in studies of the curve-crossing were removed from those solutions and rapidly transferred to fresh solutions containing electrolytes and the diiron complexes but with no added acid. Had the electrode been fouled by electrodeposition, an event at the potential of the curve crossing should have been observed. In fact, this region was completely blank.

Therefore, the curve-crossing electrochemical responses appear to be an integral property of the electroactive (−1.62 V) species, presumed to be the $Fe^IFe^I \rightarrow Fe^IFe^0$ reduction, for which a rapid chemical reaction, i.e., protonation, of the Fe^IFe^0 species produces the increased current at the more negative potential. The presence of a more easily reducible product or intermediate as seen in the reverse electrochemical scan suggests that a subsequent slow chemical reaction produces an intermediate of sufficient stability to build up in solution and migrate back to the electrode for reduction at a more positive potential. While a detailed kinetic analysis of the curve-crossing phenomenon is required to confidently relate to mechanism, an appealing presumption is that the species giving rise to the −1.28 event is a mixed valent (η^2-H_2)$Fe^{II}Fe^I$ species; its reduction releases dihydrogen and regenerates the Fe^IFe^I catalyst. Supporting this hypothesis, the EPR spectrum of a sample withdrawn from a CH_3CN/H_2O mixed solvent solution during incomplete bulk electrolysis of the dicationic complex **1-(PTA·H$^+$)$_2$** in the presence of HOAc exhibits a signal (axial with $g_{\|} = 2.016$, 2.003, 1.977 and $g_{\perp} = 1.933$) indicative of an EPR active reaction intermediate as might be associated with the expected mixed-valent species. These observations are consistent with a mechanism wherein a one-electron step at −1.62 V, followed by a one-electron reduction of a diprotonated species at −1.28 V, are involved in the electrocatalytic reaction for H_2 production in the model systems.

Mechanisms. Our results therefore point to a reductive Fe^0Fe^I route to electrocatalysis of H_2 production from phosphine-substituted (PTA and PMe_3) binuclear iron complexes in the presence of weak acid, HOAc, as a proton source. Under the same conditions, the all-CO complex **1** is an electrocatalyst only at the fully reduced Fe^0Fe^0 level, attainable at −1.95 V. Its more positive reduction potential level, producing Fe^0Fe^I, is not electrochemically active with HOAc (although it *is* with stronger acids). The asymmetric monosubstituted complex, **1-PTA**, shows electrocatalysis at its first reduction event, i.e., the Fe^0Fe^I oxidation level which at −1.54 V (in pure CH_3CN) is the most positive potential of all electrocatalysts based on **1** or its derivatives. The mechanism is presumed to be the same as for the **1-PTA$_2$** derivative, ECCE; however, the preferred site of electron-uptake (the $Fe(CO)_3$ or $Fe(CO_2)$(PTA) positions) and the preferred site for Fe^{II}−H formation are open and highly interesting issues. That is, the tricarbonyl site would more readily stabilize the Fe^0 reduced species, while the phosphine-substituted Fe would stabilize the oxidation state increase following

(26) Reich, H. J.; Cohen, M. L. *J. Org. Chem.* **1979**, *44*, 3148−3151.
(27) Houmam, A.; Hamed, E. M.; Still, I. W. J. *J. Am. Chem. Soc.* **2003**, *125*, 7258−7265.
(28) Kuchynka, D. J.; Kochi, J. K. *Inorg. Chem.* **1988**, *27*, 2574−2581.
(29) Saveant, J. M. *Acc. Chem. Res.* **1980**, *13*, 3−329.

Scheme 2. Proposed Access to the ECCE Mechanism for H_2 Production from the Fe^IFe^I Complex, **1-(PTA·H$^+$)$_2$**, and in Blue, the $Fe^{II}Fe^{II}$ Complex, **1-(μ-H)(PMe$_3$)$^+$**

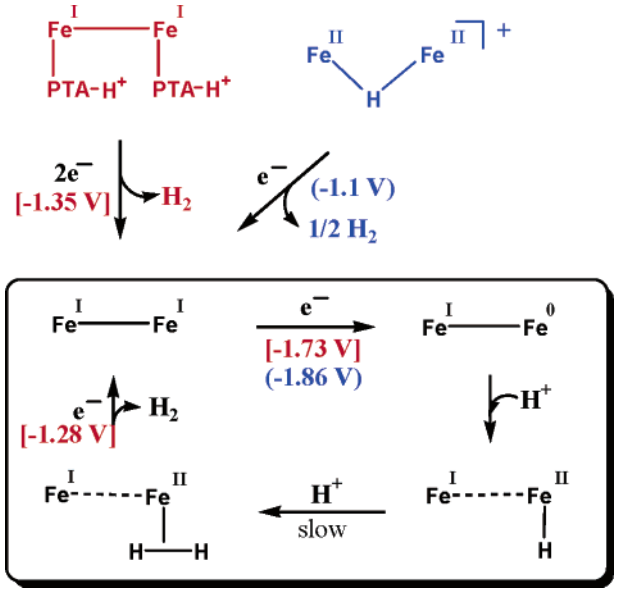

protonation and the formation of $Fe^{II}-H$ and subsequently the (η^2-H_2)Fe^{II} species.

For both the monocationic, **1-(μ-H)(PMe$_3$)$_2^+$**, and the dicationic species, **1-(PTA·H$^+$)$_2$**, the first reduction events, at −1.1 and −1.35 V, respectively, generate the Fe^I-Fe^I species from which electrocatalysis occurs, as outlined in Scheme 2. Thus, there is no apparent advantage in the synthesis of the cationic species when the weak acetic acid is to be used as a proton source as only the Fe^0Fe^I species is active in oxidative addition. When strong acids such as triflic acid are used, the more positive reduction potential of **1-(μ-H)(PMe$_3$)$_2^+$** (at −1.1 V) is catalytically active (see ref 3 and Supporting Information); however, the advantage of the more positive potential is ameliorated by the necessity for a strong acid.

Although there is no spectroscopic evidence for the (H)$Fe^{II}Fe^I$ or (η^2-H_2)$Fe^{II}Fe^I$ species proposed in the ECCE mechanism, the cathodic curve-crossing electrochemical event at −1.28 V, observed to follow reduction of **1-PTA$_2$** to the Fe^0Fe^I level, implies their existence as long-lived intermediates.

Concluding Remarks

Using the [Fe]H_2ase active site as a guide for the preparation of synthetic electrocatalysts, we and others have generated species competent for H_2 production, albeit with very low activities as compared to the [Fe]H_2ase (reported at 6000 molecules of H_2 per second per mole).[30] Nevertheless, lessons learned from these studies are convincing that low oxidation states, requiring CO as stabilizing ligand for Fe^I or Fe^0, are to be expected in biological settings. As the natural H_2-evolving electrocatalysts play reversible roles, the capability for H_2 uptake is also engineered into the protein by the presence of CN^- as a suitable ligand for Fe^{II}; CN^- has been mimicked in our studies by the PMe_3 or the PTA ligands. Notably, cyclic voltammetry studies of H_2 production with the **1-(μ-H)(PMe$_3$)$^+$** cation as the electrocatalyst found no effect of added water. Hence, we conclude that the hydrophilicity of the PTA ligand has permitted an energy gain of up to 180 mV over the PMe_3 derivatives.

The salient conclusions from the studies described above that relate to future developments of the diiron complexes as biomimetic electrocatalysts are as follows:

(1) The simple (μ-SRS)[Fe(CO)$_3$]$_2$ is precursor to a rich derivative chemistry, including modifications at the bridging thiolate and, as reported decades ago for (μ-SR)$_2$[Fe(CO)$_3$]$_2$, in CO/L substitution products.[31] This work explored CO exchange with the hydrophilic PTA ligand whose effect is to facilitate the electrocatalysis of H_2 production by ca. 0.1 to 0.2 V. Modifications of the μ-SRS at the bridgehead position, i.e., μ-S−$CH_2N(R)CH_2$−S, might be expected to provide better mimics of the enzyme active site and improve proton delivery or abstraction from an Fe^{II}-bound η^2-H_2.[7,32] Modifications of the fundamental (μ-SRS)[Fe(CO)$_2$L]$_2$ complexes are also of significance to their attachment to molecular electron sources[33] or to the surface of an electrode. Fundamental to such designs is the stability of the potential linker-complex bonds, which we have found to be disappointing in our attempts to use alkylation processes on PTA-substituted derivatives.

(2) The optimal electrocatalyst in the above study is the monosubstituted (μ-pdt)[Fe(CO)$_3$][Fe(CO)$_2$PTA], **1-PTA**, which produced H_2 at the Fe^IFe^0 redox level, achieving this at −1.54 V with HOAc as proton source in CH_3CN; even more positive values were realized in CH_3CN/H_2O mixtures: −1.4 V. It is tempting to assume that such asymmetry might stabilize the rotated square-pyramidal structure calculated to be important in both intramolecular site exchange and in ligand substitution processes,[12,34] and structurally analogous to what is present in the enzyme active site.

(3) The order of electron and proton uptake by the diiron complex, i.e., the electrochemical mechanism, is dependent on the proton delivery agent (acid or proton strength) and on the electron-richness of the proton uptake agent (the reduction potential of the catalyst). Achievement of sufficient electron density at the iron to permit protonation by a weak acid to occur may be accomplished either by the presence of good donor ligands, as in CN^- or PR_3, or by electroreduction. The presence of the PR_3 ligand pushes the reduction potential to highly negative values as contrasted to the all-CO parent complex and permits proton uptake from HOAc at the Fe^0Fe^I redox level. In the all-CO complex, the Fe^0Fe^0 level is required, which is achieved only at a similar highly negative reduction potential. Thus, electrocatalysis may occur at different oxidation levels, dependent on the extent of CO/L substitution and on acid strength leading to multiple mechanistic possibilities, ECCE, CECE, or EECC.

The diiron electrocatalyst study makes an interesting contrast to a binuclear system reported and carefully interpreted by Collman et al. a decade ago,[9] which explored electrocatalysts comprised of covalently linked porphyrin ligands containing two

(30) Adams, M. W. W. *Biochim. Biophys. Acta* **1990**, *1020*, 115−145.

(31) (a) Maresca, L.; Gregio, F.; Sbrignadello, G.; Bor, G. *Inorg. Chim. Acta* **1971**, *5*, 667−674. (b) Basato, M. *J. Chem. Soc., Dalton Trans.* **1975**, 911. (c) Aime, S.; Gervasio, G.; Rossetti, R.; Stanghellini, P. L. *Inorg. Chim. Acta* **1980**, *40*, 131. (d) Ellgen, P. C.; Gerlach, J. N. *Inorg. Chem.* **1973**, *12*, 2526−2532.

(32) Lawrence, J. D.; Li, H.; Rauchfuss, T. B.; Bénard, M.; Rohmer, M.-M. *Angew. Chem., Int. Ed.* **2001**, *40*, 1768−1771.

(33) Ott, S.; Kritikos, M.; Åkermark, B.; Sun, L. *Angew. Chem., Int. Ed.* **2003**, *42*, 3285−3288.

(34) Georgakaki, I. P.; Thomson, L. M.; Lyon, E. J.; Hall, M. B.; Darensbourg, M. Y. *Coord. Chem. Rev.* **2003**, *238*−*239*, 255−266.

face-to-face Ru or Os metal ions. They observed, as did we, that both the reduction potential of the dinuclear complex and the strength of the acid or proton source determined the overvoltage for H_2 production. In both systems, two redox levels are achievable; with weak acids H_2 is produced at the more negative level. Collman et al. concluded that minor modifications in the porphyrin ligands that supported the redox levels $Ru^{III-III/III-II}$ and $Ru^{III-II/II-II}$ could not effect a significant lowering of the overvoltage for H_2 production. Both studies addressed electrochemical mechanisms, with the Collman study concluding that a single-site metal protonation (yielding a η^2-H_2 complex of Ru^{IV} or Os^{IV}) was equally possible to a dimetal hydride in which two cofacial M^{III} hydrides work in concert to eliminate H_2.[9]

It is our contention that the electrocatalytic ability of the diiron H_2ase model complexes is best accommodated by successive protonation of a single Fe^0 yielding an (η^2-H_2)Fe^{II} complex of well-established precedent. In this view of the binuclear complex, the pendant $Fe(CO)_2L(pdt)$ unit serves as a four-electron donor ligand to the $Fe^{II}(\eta^2$-$H_2)$ species much in the same way a classical diphosphine ligand would stabilize such H−Fe^{II} and (η^2-H_2)Fe^{II} complexes as have been characterized by Morris et al.[35] This analogy is presented below in eqs 2 and 3. A further indication that a single metal site is sufficient for H_2 evolution comes from mononuclear Fe porphyrins shown to evolve H_2 from protons at the Fe^0 level.[36]

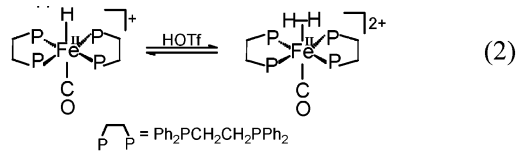

(2)

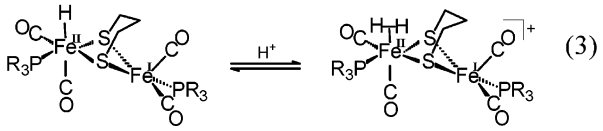

(3)

While the proposed hydrogen-containing species of eq 3 have not been isolated as stable molecules, at least an indication of the existence of the η^2-H_2 complex has possibly developed in the form of "curve-crossing" phenomenon noted in Figure 8. Furthermore, the proposed (η^2-H_2)$Fe^{II}Fe^{I}$ species is analogous to Pickett's mixed-valent $Fe^{II}Fe^{I}(S'_3)Fe_2(CO)_4(CN)_2^-$ complex, where a CO has replaced the η^2-H_2 moiety, which was generated electrochemically and characterized by IR and EPR spectroscopies.[37] Assuming the correctness of this analogy, a successful synthetic effort into the isolation of a binuclear η^2-H_2Fe^{II} complex may be feasible and is worth pursuing.

Acknowledgment. We acknowledge financial support from the National Science Foundation (Grants CHE-01-11629 to M.Y.D. for this work and CHE-0092010 for the EPR instrument) and contributions from the R. A. Welch Foundation. The X-ray diffractometers and crystallographic computing systems in the X-ray Diffraction Laboratory at the Department of Chemistry, Texas A&M University were purchased from funds provided by the National Science Foundation. Helpful discussions with Professor Donald Darensbourg are gratefully acknowledged. We also thank Prof. D. Darensbourg's research group for providing the PTA ligand. Dr. Matthew L. Miller, a former member of our group, solved the crystal structure of **1-PTA$_2$**. R.M.R. gratefully acknowledges the Universidad Autonoma de Queretaro and PROMEP for their support.

Supporting Information Available: Molecular structure and X-ray crystallographic tables for complexes **1-PTA** and **1-PTA$_2$**. In situ spectroelectrochemical data for **1-(PTA·H$^+$)$_2$** (CIF, PDF). This material is available free of charge via the Internet at http://pubs.acs.org.

JA039394V

(35) Forde, C. E.; Landau, S. E.; Morris, R. H. *J. Chem. Soc., Dalton Trans.* **1997**, 1663−1664.
(36) Bhugun, I.; Lexa, D.; Savéant, J.-M. *J. Am. Chem. Soc.* **1996**, *118*, 3982−3983.
(37) Razavet, M.; Borg, S. J.; George, S. J.; Best, S. P.; Fairhurst, S. A.; Pickett, C. J. *Chem. Commun.* **2002**, 700−701.